Trace-element geochemistry and S–O isotopes in the fluorite-barite mineralization of Merguechoum, Moroccan eastern Meseta: insights into ore genesis to the Pangea rifting

Mohammed Cherai[1] · Larbi Rddad[2] · Fouad Talbi[1] · Benjamin F. Walter[3,4]

Abstract The Merguechoum fluorite-barite mineralization, located in the Eastern Meseta of Morocco, is hosted in the Late Hercynian granite. The ore consists of fine crystals of fluorite 1, massive barite 1, euhedral crystals of fluorite 2, and barite 2 with calcite and minor quartz and sulfides. The Merguechoum ore deposits have never been investigated. This study was the first contribution that studied the genesis of fluorite and barite. The ore occurs as dissemination within granite intrusion and also fills the NE-SW-trending meter-sized fractures and faults. The values of the total Rare Earth Elements and Yttrium (REY) and the ratios of LREY/HREY, Y/Ho, Tb/Ca, and Tb/La indicate that the Merguechoum fluorite precipitated from hydrothermal fluids, likely basinal brines, which interacted with the Hercynian granite. The REY data indicate that the ore-forming fluids of the early stage have intensely interacted with the Hercynian granite compared to those of the late ore stage. The gradual decrease in the europium (Eu/Eu*), yttrium (Y/Y*), and cerium (Ce/Ce*) anomalies and a low concentration of ΣREY observed in the second ore stage compared to the first ore stage suggest an increase in pH and fO_2 and by inference a decrease in temperature during the evolution of the hydrothermal system. This evolution could be explained by fluid mixing between the ascending basinal hydrothermal fluids and the diluted sulfate-rich meteoric water barite separates from selected samples reveal that the dissolved sulfates (SO_4^{2-}) were derived from Permian Triassic sulfates and/or coeval pore-seawater sulfates. The proposed fluid mixing triggered the precipitation of an early-stage F-Ba assemblage followed by the second-stage F-Ba mineralization. Geologic fieldwork, REY inventories, and isotope data point to the ore genesis during the Permian Triassic extensional tectonic activity concerning the Pangea rifting. This extensional tectonic environment is likely the driving force that mobilized a large amount of the ore-forming basinal brines along the available faults and fractures to the loci of ore deposition.

Keywords Fluorite-barite veins · Geochemistry of REY and trace elements · O S isotopes · Late hercynian granite · Pangea rifting · Merguechoum · Eastern Meseta of Moroccan

✉ Mohammed Cherai
cheraibg@gmail.com

[1] Faculté des Sciences, Laboratoire de Géosciences, Géo Environnement et Prospection Minière et Hydrique, BP 717, 60000 Oujda, Maroc

[2] Earth and Planetary Science Division, Physical Science Department, Kingsborough Community College of the City University of New York (CUNY), 2001 Oriental Boulevard, Brooklyn, NY 11235 2398, USA

[3] Chair of Economic Geology and Geochemistry, Karlsruhe Institute of Technology (KIT), Adenauerring 20B, 76131 Karlsruhe, Germany

[4] Laboratory for Environmental and Raw Material Analyses (LERA), Adenauerring 20B, 76131 Karlsruhe, Germany

1 Introduction

Several economic vein-type fluorite-barite ore deposits of economic values are commonly associated with carbonatites (Okoruso, Namibia; Amba Dongar, India), granitic breccias (Vergenoeg, Republic South Africa), or related to basinal brines, typical of the Mississippi-Valley-Type (MVT) ore deposits (González-Partida et al. 2003; Munoz

et al. 2005; Bouabdellah et al. 2016; Nadoll et al. 2019a). In these ore deposits, fluorite precipitated from i) hydrothermal-magmatic fluids that are related to igneous rock intrusions (Gallinas Mountains et al. 2000), (ii) mixing between meteoric water and carbonatite-derived fluid (Amba Dongar, India; Simonetti and Bell 1995) or (iii) basinal brines typically of MVT systems (e.g. the Lower Harz Mts., Schwarzwald and Ore Mountains, Germany; Alles et al. 2019; de Graaf et al. 2020; Walter et al. 2019; Haschke et al. 2021).

In Morocco, fluorite ore deposits were investigated in the eastern Meseta (e.g. Aouli fluorite-barite ore deposits, Margoum et al. 2015). The fluorite-barite ore of Aouli, hosted in the Hercynian granite, was formed because of the mixing between a hot ascending deep-seated basinal brine and cooler, diluted formational and or meteoric water in relation to the Pangea rifting (Margoum et al. 2015; Burisch et al. 2022). The Merguechoum fluorite-barite ore, located in the eastern Moroccan Meseta, is also hosted in the Hercynian granite, and shares similar geological characteristics as the Aouli ore deposits. This contribution seeks to find out whether the Merguechoum fluorite-barite ore was formed to the basinal brines or the Hercynian magmatic-derived fluids with or without the involvement of meteoric water.

The Jbel Merguechoum is composed of a Late Hercynian granite (321 ± 15 Ma) (El Hadi et al. 2003) with a potassium-alkaline affinity (Hollard 1978; Hoepffner 1987; Gasquet et al. 1996; El Hadi et al. 2003). This intensely fractured granite hosts the structurally controlled fluorite-barite ore, which consists of abundant fluorite and barite minerals that are associated with calcite with subordinate chalcopyrite and pyrite. The formation of these ore deposits within granite raises the possible role of the granitic magma in the genesis of fluorite. REY geochemistry is widely used to help constrain the origin and the geological environment of fluorite and barite mineralization in several ore deposits (Möller et al. 1976; Bau et al. 2003; Schwinn and Markl 2005; Sasmaz and Yavuz 2007; Schönenberger et al. 2008; Souissi et al. 2010; Ehya 2012; Akgul 2015; Alipour et al. 2015; Azizi et al. 2017; Kraemer et al. 2019). In this current study, mineralogical and geochemical analyses were performed on the ore and gangue minerals encompassing the paragenetic sequence as well the host rock (i.e. granite) for the first time to shed light on i) the source of the ore-forming fluids and ii) the evolution of the hydrothermal fluids involved in the genesis of fluorite. Upon combining the geological field data with the geochemical and mineralogical data, a genetic model for the ore emplacement was established.

Table 1 Paragenetic sequence of fluorite barite mineralization stages of Jbel Merguechoum

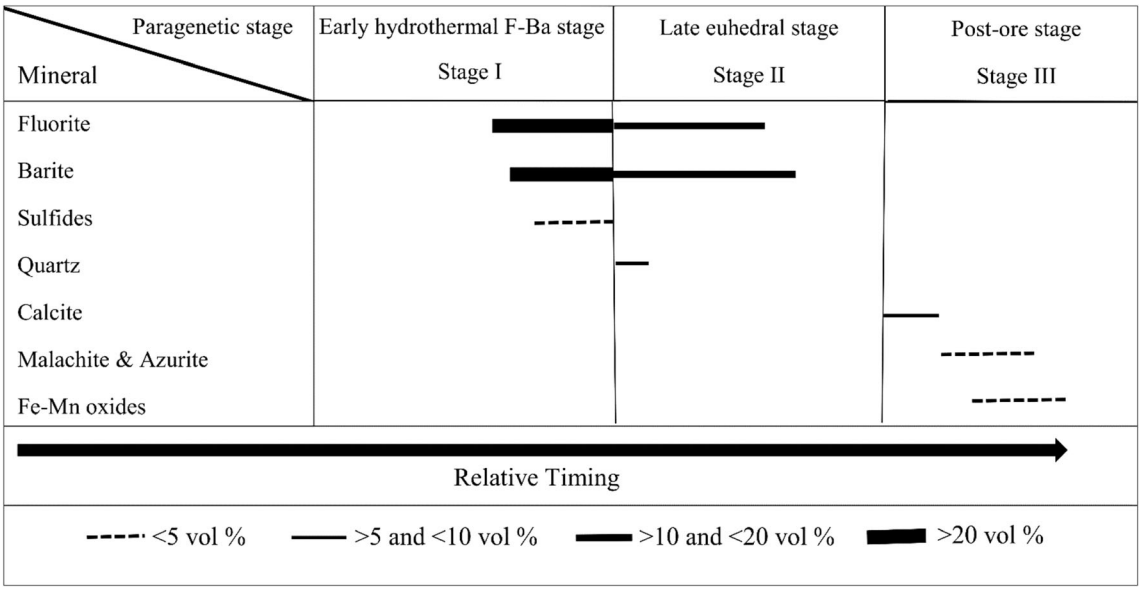

Table 2 Concentrations of rare earth and trace elements in Jbel Merguechoum (ppm)

Type	Massive fluorite (F-1)								Euhedral fluorite (F-2)					
No	Green Fluorite 1	Green Fluorite 2	White Fluorite	Blue Fluorite	Colorless Fluorite	Purle Fluorite	Green- Purple Fluorite	Average (n = 7)	Blue Fluorite 1	Blue Fluorite 2	Green Fluorite	Purple Fluorite 1	Purple Fluorite 2	Average (n = 5)
Ca	500,000	500,000	400,000	570,000	650,000	550,000	500,000	524,285 71	400,000	400,000	450,000	450,000	550,000	450,000
Li	0 10	0 20	0 60	0 40	0 20	0 10	1 70	0 47	0 60	0 10	0 10	0 20	0 10	0 22
Be	1 00	0 80	1 00	1 00	1 00	0 80	0 80	0 91	1 00	1 00	1 00	0 90	1 00	0 98
V	1 00	1 00	1 00	0 90	1 00	1 00	0 70	0 94	0 70	0 70	0 70	3 00	0 90	1 20
Sc	0 10	0 09	0 06	0 30	0 10	0 10	0 09	0 12	0 09	0 07	0 09	0 08	0 06	0 08
Cr	0 80	0 80	0 90	1 00	1 00	1 00	1 00	0 93	1 00	0 70	0 90	0 80	1 00	0 88
CO	0 20	0 20	0 20	0 20	0 10	0 10	0 20	0 17	0 10	0 09	0 20	0 01	0 10	0 10
Ni	0 10	1 60	1 00	2 50	1 50	0 10	1 10	1 13	0 10	0 10	3 80	0 50	0 10	0 92
Cu	22 40	12 60	3 80	4 10	3 00	1 00	1 30	6 89	7 00	0 10	19 70	8 80	1 30	7 38
Zn	1 30	1 40	2 00	1 40	1 20	0 80	2 30	1 49	1 70	0 40	0 90	1 80	0 70	1 10
Ga	0 02	0 04	0 02	0 02	0 02	0 02	0 01	0 02	0 09	0 01	0 05	0 08	0 04	0 05
Rb	0 10	0 10	0 20	0 10	0 10	0 10	0 20	0 13	0 10	0 03	0 10	0 60	0 10	0 19
K	90 00	100 00	100 00	70 00	50 00	70 00	30 00	72 86	90 00	90 00	90 00	100 00	100 00	94 00
Sr	10 00	32 00	39 00	14 00	7 00	70 00	12 00	26 29	23 25	16 03	30 90	75 00	60 00	41 04
Y	17 40	57 50	68 80	89 50	73 10	4 60	65 50	53 77	0 60	0 50	20 30	6 10	5 90	6 68
Zr	0 10	0 20	0 20	0 09	0 09	0 10	0 06	0 12	0 09	0 08	0 06	0 40	0 09	0 14
Nb	0 09	0 08	0 09	0 11	0 11	0 09	0 06	0 09	0 04	0 04	0 09	0 16	0 08	0 08
Cs	0 05	0 01	0 05	0 10	0 03	0 02	0 06	0 05	0 03	0 00	0 02	0 06	0 09	0 04
Ba	146 00	1431 00	1134 00	179 00	59 00	2150 00	58 00	736 71	452 00	689 00	1092 00	3059 00	1795 00	1417 40
La	3 50	3 70	3 10	0 70	3 10	1 00	3 20	2 61	0 20	0 10	3 80	2 40	0 90	1 48
Ce	4 46	6 36	6 60	1 40	4 52	1 27	5 40	4 29	0 21	0 10	5 79	1 90	1 51	1 90
Pr	0 60	0 80	0 80	0 30	0 50	0 20	0 90	0 59	0 02	0 01	0 80	0 60	0 30	0 35
Nd	1 50	4 30	4 50	1 40	2 20	0 70	4 10	2 67	0 10	0 05	3 20	2 10	1 10	1 31
Sm	0 30	1 30	1 80	0 80	0 40	0 20	1 60	0 91	0 03	0 02	0 50	0 40	0 20	0 23
Eu	0 03	0 30	0 50	0 20	0 03	0 02	0 50	0 23	0 00	0 00	0 05	0 07	0 03	0 03
Gd	0 30	1 70	3 00	1 80	0 30	0 10	2 80	1 43	0 03	0 02	0 40	0 30	0 09	0 17
Tb	0 09	0 20	0 40	0 30	0 08	0 02	0 40	0 21	0 01	0 01	0 09	0 05	0 02	0 03
Dy	0 30	1 50	2 60	2 80	0 50	0 10	2 80	1 51	0 04	0 04	0 50	0 20	0 09	0 17
Ho	0 08	0 30	0 50	0 60	0 10	0 02	0 50	0 30	0 01	0 01	0 08	0 05	0 02	0 03
Er	0 20	0 80	1 40	1 80	0 60	0 06	1 40	0 89	0 03	0 04	0 20	0 10	0 07	0 09
Tm	0 03	0 08	0 10	0 20	0 07	0 01	0 20	0 10	0 01	0 01	0 03	0 02	0 01	0 01
Yb	0 10	0 40	0 80	1 00	0 40	0 20	0 70	0 51	0 04	0 05	0 10	0 20	0 20	0 12
Lu	0 02	0 07	0 10	0 10	0 08	0 03	0 09	0 07	0 01	0 01	0 02	0 03	0 03	0 02
Hf	0 02	0 02	0 02	0 01	0 01	0 02	0 02	0 02	0 02	0 02	0 01	0 01	0 02	0 02
Ta	0 03	0 03	0 10	0 04	0 09	0 09	0 09	0 07	0 10	0 01	0 05	0 09	0 10	0 07
Ti	10 00	10 00	10 00	10 00	10 00	6 00	5 00	8 71	10 00	8 00	90 00	20 00	8 00	27 20
Pb	0 58	4 50	6 99	4 23	0 67	1 86	1 92	2 96	0 72	0 07	1 87	22 92	0 78	5 27

Table 2 continued

Type	Massive fluorite (F-1)								Euhedral fluorite (F-2)					
No	Green Fluorite 1	Green Fluorite 2	White Fluorite	Blue Fluorite	Colorless Fluorite	Purle Fluorite	Green- Purple Fluorite	Average (n = 7)	Blue Fluorite 1	Blue Fluorite 2	Green Fluorite	Purple Fluorite 1	Purple Fluorite 2	Average (n = 5)
Bi	0 06	0 59	0 03	0 04	0 05	0 04	0 23	0 15	0 04	0 03	0 04	0 01	0 03	0 03
Th	0 10	0 10	0 10	0 10	0 10	0 10	0 10	0 10	0 10	0 10	0 10	0 09	0 10	0 10
U	0 09	0 10	0 10	0 08	0 20	0 09	0 08	0 11	0 10	0 09	0 20	0 07	0 09	0 11
P	10 00	8 00	9 00	10 00	10 00	10 00	10 00	9 57	9 00	5 00	9 00	7 00	10 00	8 00
REE	11 51	21 81	26 20	13 40	12 88	3 93	24 59	16 33	0 73	0 46	15 56	8 42	4 57	5 95
LREE	10 39	16 76	17 30	4 80	10 75	3 39	15 70	11 30	0 56	0 28	14 14	7 47	4 04	5 30
HREE	1 12	5 05	8 90	8 60	2 13	0 54	8 89	5 03	0 17	0 18	1 42	0 95	0 53	0 65
LREE/ HREE	9 28	3 32	1 94	0 56	5 05	6 28	1 77	4 03	3 29	1 58	9 99	7 86	7 62	6 07
(La/ Yb)n	25 11	6 64	2 78	0 50	5 56	3 59	3 28	6 78	3 59	1 43	27 26	8 61	3 23	8 82
(La/ Ho)n	10 45	2 95	1 48	0 28	7 40	11 94	1 53	5 15	4 78	2 39	11 34	11 46	10 75	8 14
La/Ho	43 75	12 33	6 20	1 17	31 00	50 00	6 40	21 55	20 00	10 00	47 50	48 00	45 00	34 10
Y/Ho	217 50	191 67	137 60	149 17	731 00	230 00	131 00	255 42	60 00	50 00	253 75	122 00	295 00	156 15
(La/ Nd)n	4 60	1 70	1 36	0 99	2 78	2 81	1 54	2 25	3 94	3 94	2 34	2 25	1 61	2 82
(Gd/ Yb)n	2 48	3 52	3 10	1 49	0 62	0 41	3 31	2 13	0 62	0 33	3 31	1 24	0 37	1 17
Eu/Eu*	0 30	0 62	0 65	0 49	0 25	0 38	0 72	0 49	0 30	0 30	0 33	0 59	0 59	0 42
Ce/Ce*	0 69	0 86	0 87	0 75	0 81	0 66	0 77	0 77	0 65	0 62	0 77	0 38	0 71	0 63
Y/Y*	8 54	6 54	4 60	5 27	24 93	7 84	4 20	8 85	2 29	1 91	7 65	4 65	10 62	5 42

Type	Massive Calcite			Crystal Quartz			Late hercynian granite			
No	White calcite 1	White Calcite 2	Average (n = 2)	White-Purple Quartz	White Quartz	Average (n = 2)	G1	G2	G3	Average (n = 3)
Ca	400,000	400,000	400,000	400	600	500	2700	2800	15,200	6900
Li	0 10	0 10	0 10	17 70	20 20	18 95	103 40	106 30	81 70	97 13
Be	1 00	0 70	0 85	0 90	0 70	0 80	3 00	2 00	4 00	3 00
V	0 80	1 00	0 90	1 00	1 00	1 00	58 00	51 00	66 00	58 33
Sc	0 09	0 10	0 10	0 10	0 09	0 10	4 40	4 70	9 40	6 17
Cr	1 00	0 80	0 90	1 00	0 80	0 90	6 00	6 00	8 00	6 67
Co	0 10	0 40	0 25	0 07	0 10	0 09	0 80	1 30	7 90	3 33
Ni	0 20	0 30	0 25	0 10	0 10	0 10	2 50	2 20	5 40	3 37
Cu	5 10	3 20	4 15	5 30	0 50	2 90	133 70	81 30	7 30	74 10
Zn	1 30	1 00	1 15	3 40	1 60	2 50	26 10	26 90	43 50	32 17
Ga	0 03	0 01	0 02	0 04	0 01	0 03	17 73	17 42	16 52	17 22

Table 2 continued

Type	Massive Calcite			Crystal Quartz			Late hercynian granite			
No	White calcite 1	White Calcite 2	Average (n = 2)	White-Purple Quartz White Quartz Average		(n = 2)	G1	G2	G3	Average (n = 3)
Rb	0 20	0 10	0 15	1 10	0 40	0 75	256 10	250 70	228 90	245 23
K	0 01	0 01	0 01	0 01	0 01	0 01	55,400 00	53,600 00	45,900 00	51,633 33
Sr	20 39	25 35	22 87	6 00	6 00	6 00	99 00	101 00	342 00	180 67
Y	0 08	0 09	0 09	0 10	0 10	0 10	22 90	20 10	22 80	21 93
Zr	0 20	0 09	0 15	0 20	0 20	0 20	39 50	43 30	51 00	44 60
Nb	0 04	0 03	0 04	0 04	0 02	0 03	7 93	12 04	12 28	10 75
Cs	0 10	0 10	0 10	0 20	0 10	0 15	22 80	24 10	11 90	19 60
Ba	607 00	515 00	561 00	109 00	139 00	124 00	398 00	428 00	918 00	581 33
La	0 06	0 02	0 04	0 01	0 08	0 04	25 10	42 70	62 90	43 57
Ce	0 05	0 02	0 04	0 01	0 11	0 06	51 35	71 08	115 81	79 41
Pr	0 00	0 00	0 00	0 00	0 00	0 00	6 30	10 60	12 60	9 83
Nd	0 02	0 02	0 02	0 01	0 02	0 02	22 90	37 60	41 60	34 03
Sm	0 01	0 01	0 01	0 01	0 01	0 01	4 60	7 10	6 60	6 10
Eu	0 00	0 00	0 00	0 00	0 00	0 00	1 10	1 40	1 40	1 30
Gd	0 01	0 01	0 01	0 01	0 01	0 01	3 90	4 70	5 80	4 80
Tb	0 00	0 00	0 00	0 00	0 00	0 00	0 50	0 70	0 70	0 63
Dy	0 01	0 01	0 01	0 01	0 01	0 01	3 40	3 60	4 90	3 97
Ho	0 00	0 00	0 00	0 00	0 00	0 00	0 80	0 60	0 90	0 77
Er	0 01	0 01	0 01	0 01	0 01	0 01	1 90	1 80	2 70	2 13
Tm	0 00	0 00	0 00	0 00	0 00	0 00	0 30	0 30	0 40	0 33
Yb	0 01	0 01	0 01	0 01	0 01	0 01	2 00	2 00	2 60	2 20
Lu	0 00	0 00	0 00	0 00	0 00	0 00	0 30	0 30	0 40	0 33
Hf	0 01	0 01	0 01	0 02	0 01	0 02	1 54	1 99	2 02	1 85
Ta	0 10	0 07	0 09	0 05	0 05	0 05	0 70	1 20	1 20	1 03
Ti	5 00	8 00	6 50	5 00	9 00	7 00	229,000 0	201,000 0	228,000 0	219,333 3
Pb	0 63	0 36	0 50	0 56	0 70	0 63	15 63	17 31	31 30	21 41
Bi	0 02	0 02	0 02	0 03	0 03	0 03	0 59	0 10	0 23	0 31
Th	0 08	0 05	0 07	0 08	0 06	0 07	30 10	37 20	38 60	35 30
U	0 10	0 09	0 10	0 07	0 10	0 09	8 50	8 10	6 60	7 73
P	10 00	8 00	9 00	8 00	10 00	9 00	910 00	940 00	780 00	876 67
REE	0 17	0 11	0 14	0 07	0 25	0 16	124 45	184 48	259 31	189 41
LREE	0 13	0 07	0 10	0 03	0 22	0 13	111 35	170 48	240 91	174 25
HREE	0 04	0 04	0 04	0 03	0 03	0 03	13 10	14 00	18 40	15 17
LREE/HREE	3 64	1 92	2 78	1 02	6 68	3 85	8 50	12 18	13 09	11 26
(La/Yb)n	4 78	1 79	3 29	0 82	8 20	4 51	9 00	15 31	17 35	13 89
(La/Ho)n	7 16	2 39	4 78	0 96	9 55	5 25	7 49	17 00	16 69	13 73

Table 2 continued

Type	Massive Calcite			Crystal Quartz			Late hercynian granite			
No	White calcite 1	White Calcite 2	Average (n = 2)	White-Purple Quartz	White Quartz	Average (n = 2)	G1	G2	G3	Average (n = 3)
La/Ho	30 00	10 00	20 00	4 00	40 00	22 00	31 38	71 17	69 89	57 48
Y/Ho	40 00	45 00	42 50	50 00	50 00	50 00	28 63	33 50	25 33	29 15
(La/Nd)n	7 88	1 97	4 93	1 58	7 88	4 73	2 16	2 24	2 98	2 46
(Gd/Yb)n	0 64	0 83	0 74	0 71	0 71	0 71	1 61	1 94	1 85	1 80
Eu/Eu*	0 38	0 37	0 37	0 39	0 39	0 39	0 77	0 70	0 68	0 72
Ce/Ce*	0 57	0 56	0 57	0 54	0 95	0 74	0 97	0 80	0 95	0 91
Y/Y*	1 44	1 62	1 53	1 80	1 80	1 80	1 06	1 03	0 83	0 97

The equations used to calculate Eu, Ce, and Y anomalies are Eu/Eu^* $Eu_N/[(Sm_N + Gd_N)/2]$, Ce/Ce^* $Ce_N/[(La_N + Pr_N)/2]$, and Y/Y^* $Y_N/[(Dy_N + Ho_N)/2]$ (after Deng et al 2014)

2 Geological setting

2.1 Lithostratigraphy

In the Jbel Merguechoum, the Triassic and Liassic rocks are exposed to the surface, whereas the Paleozoic sequence is hidden beneath the Mesozoic series, except for the exhumation of the Late Hercynian granite (Figs. 1 and 2). The rest of the Paleozoic series consists of metasedimentary and/or volcano-sedimentary formations (Giret 1985). Petrographically, the Merguechoum granite consists of two major petrographic units; leucocratic granite with a coarse-grained texture and quartz monzonites with a porphyritic texture (Berrada-Hmima 1993; El Hadi et al. 2003). These granitoids are characterized by the predominance of euhedral to subhedral alkali feldspar phenocrysts and anhedral quartz crystals with the subordinate plagioclase, amphibole, and biotite (Berrada-Hmima 1993; El Hadi et al. 2003). The Triassic sequence (10 1000 m) consists of red-bed siltstone and evaporite-bearing argillites that are locally intercalated with tholeiitic basalts. These Triassic series are dominantly exhumed in the west of the Jbel Merguechoum area where they are covered by a 180 m-thick Liassic carbonate. The overlying Middle Jurassic formation, encountered in the east and west of Jbel Merguechoum, consists of a carbonate (dolostone and limestone) platform with marl intercalations. The Quaternary cover consists of conglomerates, sandy clays, and other fluvio-alluvial sediments.

2.2 Tectonic evolution

The Palaeozoic basement of the Eastern Meseta forms small inliers (Merguechoum, Jerada, Zekkara, and Tancherfi) and is overlain by the Mesozoic sedimentary cover. The tectonic evolution of the Jbel Merguechoum is part of the Moroccan Hercynian geodynamic history that occurred between 330 and 270 Ma (Lagard 1989). The structural evolution of the Eastern Meseta of Morocco, including Jebel Merguechoum, is dominated by regional strike-slip faults, which formed as a result of a succession of the two major tectonic events: the Hercynian and the Alpine orogenies.

The Hercynian orogeny consists of two major tectonic events (Clauer et al. 1980; Huon et al. 1987): (i) the Eo-Variscan phase (366 372 Ma) and (ii) the Late Hercynian phase (286 and 247 Ma) (Mrini et al. 1992). The former tectonic event was responsible for the generation of the NNE SSW, N S, and NW SE-trending faults. The latter tectonic event resulted in the emplacement of numerous granites (e.g., Merguechoum, Tancherfi) and the formation of the NE SW- to E-W-trending faults (Hoepffner et al.

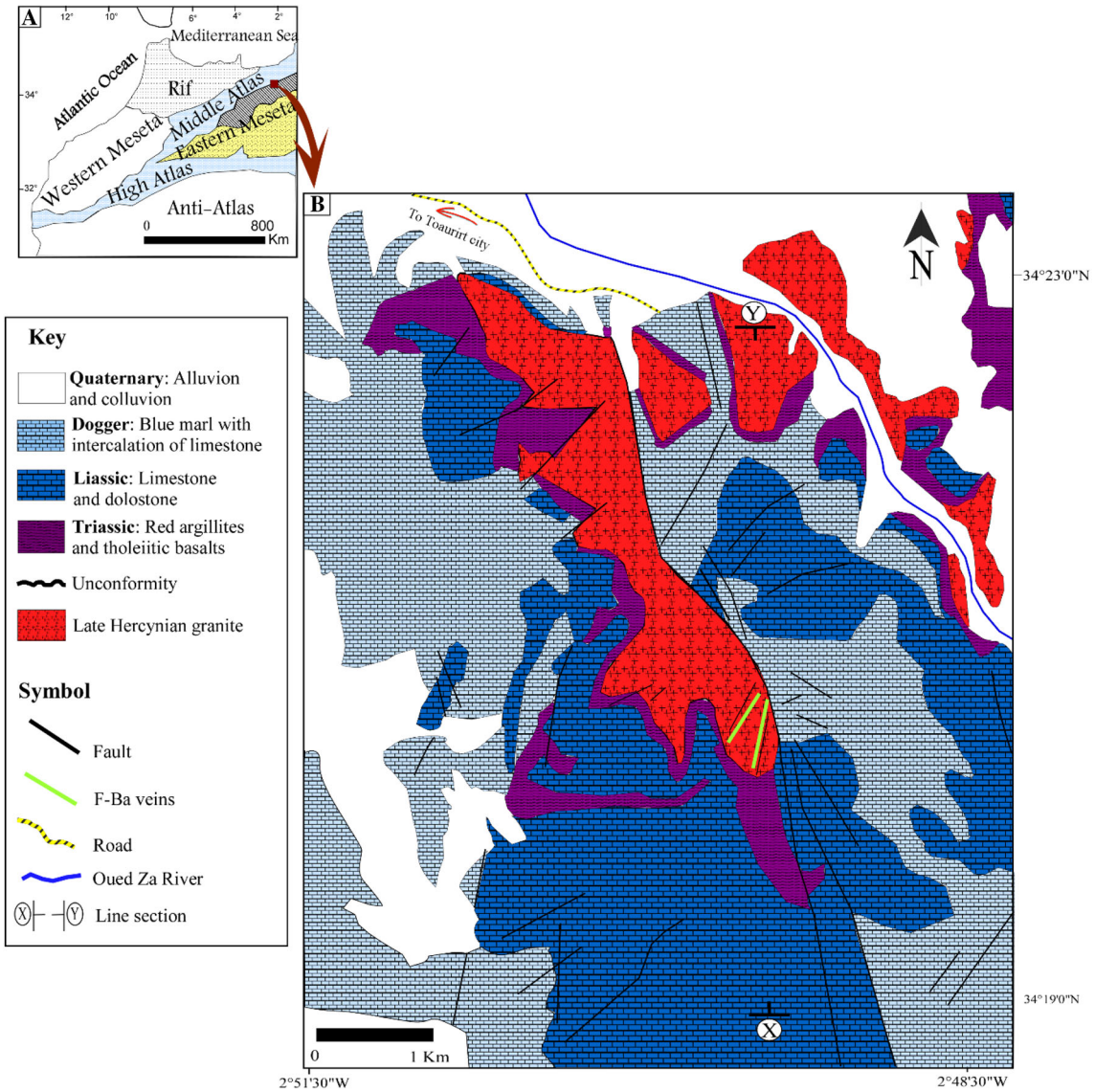

Fig. 1 **A** General location of Merguechoum inlier. **B** Generalized geologic map of the Jbel Merguechoum showing the local geology, major faults, and the location of the mineralized NE SW trending veins (from the Taourirt geological map at 1/50000; modified)

2005). These Hercynian structures were affected by the Triassic Jurassic extensional tectonic activities which are particularly characterized by the development of the NE-SW- to ENE WSW-trending normal faults (Hoepffner et al. 2005). During the Cretaceous to Quaternary, the Eastern Meseta underwent the Alpine compressive events, which resulted in the formation of the NNE SSW- and NW SE-trending structures (Chotin et al. 2000; Torbi and Gélard 2000) and the uplift of the present-day Jbel Merguechoum.

2.3 Ore geology

Petrographic examination and crosscutting relationships between different mineral phases allow the identification of a simple paragenetic sequence with three main stages (Table 1). The early hydrothermal stage (Stage I) comprises the main economic ore accounting for more than 90% of total fluorite-barite resources. All varieties of fluorite minerals are represented in this stage I, except the subhedral blue fluorite. The mineral paragenesis consists of early fluorite (F-1), purple massive barite (Ba-1), euhedral fluorite (F-2), lamellar barite (Ba-2) associated with calcite, and quartz with subordinate sulfides (pyrite, chalcopyrite).

Early fluorite (F-1) is massive, greenish, colorless, or white, and locally it may have oscillatory zoning. Fluorite 1 occurs also as metasomatic mineralization due to the progressive replacement of Late Hercynian granite by fluorite 1. The latter forms subhedral to anhedral microcrystalline crystals (< 5 mm) of various morphology (Fig. 3E). Barite

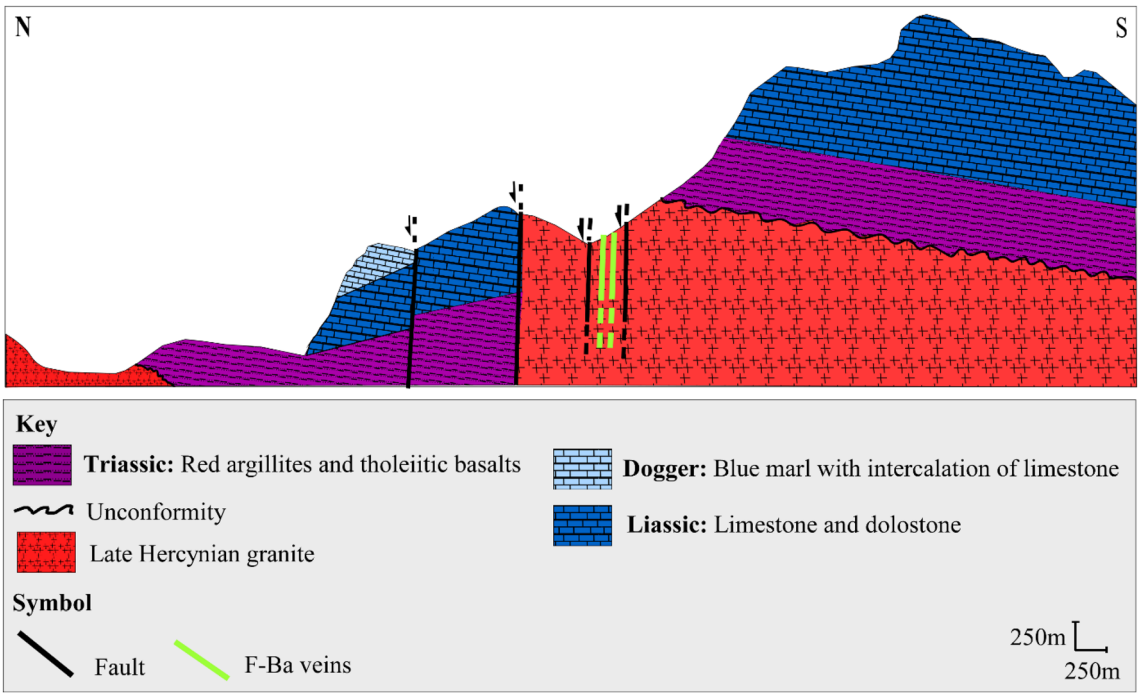

Fig. 2 Representative N S cross section through the Jbel Merguechoum fluorite barite veins showing the major lithostratigraphic units and the location of the main fluorite barite veins (see the map of, Fig. 1 for the location of the X Y line)

1 occurs as white to pink massive white to transparent crystals, which are associated with early fluorite.

The second hydrothermal stage (Stage II, ·Euhedral stagë) is characterized by well-developed crystals. It consists of cm-sized cubes of green, blue, and purple fluorite (F-2), white to transparent barite (Ba-2), and white to light purple pyramid quartz crystals.

Calcite is also present as a massive mineral crosscutting the Late Hercynian granite. Sulfides are rare and consist of small amounts of chalcopyrite and pyrite disseminated within the Late Hercynian granite The post-ore-stage (Stage III) comprises a supergene mineral assemblage and calcite. It consists of Fe Mn oxides-hydroxides and traces of malachite and azurite disseminated in granite.

Based on field observations of the fluorite-barite ore, two main ore styles can be distinguished: (i) open space-filling that was tectonically controlled and (ii) metasomatic replacement. Open space-filling ore is predominant and is represented by veins, veinlets, geodes, and en echelon tension gash clusters in fracture zones in the Merguechoum granitic intrusion (Figs. 2, 3A F). The mineralized NNE-SSW- to NE-SW- trending veins consist of a complex system of sub-vertical veins (85 degree dipping to the North) that extend up to 700 m in length with a thickness that can reach up to 1 m. These veins are parallel to the regionally reactivated Hercynian faults.

3 Sampling and analytical method

Minerals encompassing the paragenetic sequence were collected from different ore styles, colors, and morphologies. Representative samples of fluorite (n = 12), barite (n = 4), calcite (n = 2), quartz (n = 2), and fresh Hercynian granite (n = 3) were collected. All sampled rocks and minerals were crushed using agate mortars and carefully handpicked under a binocular microscope to avoid contamination.

The selected materials were then crushed to a size of 200 mesh for trace elements and REY analysis by the Inductively Coupled Plasma Mass Spectrometry (ICP-MS) at Bureau Veritas Minerals (Canada) using an ELAN 9000 ICP-MS type apparatus for samples of fluorite, (MPF, MWF, MGF1, CPF1, CBF1) barite (MPB, MWB, CTB, CWB), calcite (MWC1), quartz (CWQ), and granite (G1, G2, G3). At the Geochemistry Lab of Jacobs University Bremen, Germany, samples of fluorite (MTF, MBF, MGF2, CGF, CBF2, CPF2), calcite (MWC2), and quartz (CPWQ) were analyzed for trace elements and REY using the quadrupole ICP-MS. 30 mg of powdered samples were digested in a mixture of (2:2:1:1) H_2O-HF-$HClO_4$-HNO_3, 50% HCl for one hour. In Bremen, the samples were digested for 12 h at elevated temperatures with HF-HNO_3-HCl in a Picotrace DAS digestion unit with pressure-sealed PTFE bombs. The solutions were evaporated to incipient dryness and redissolved in concentrated HCl twice before

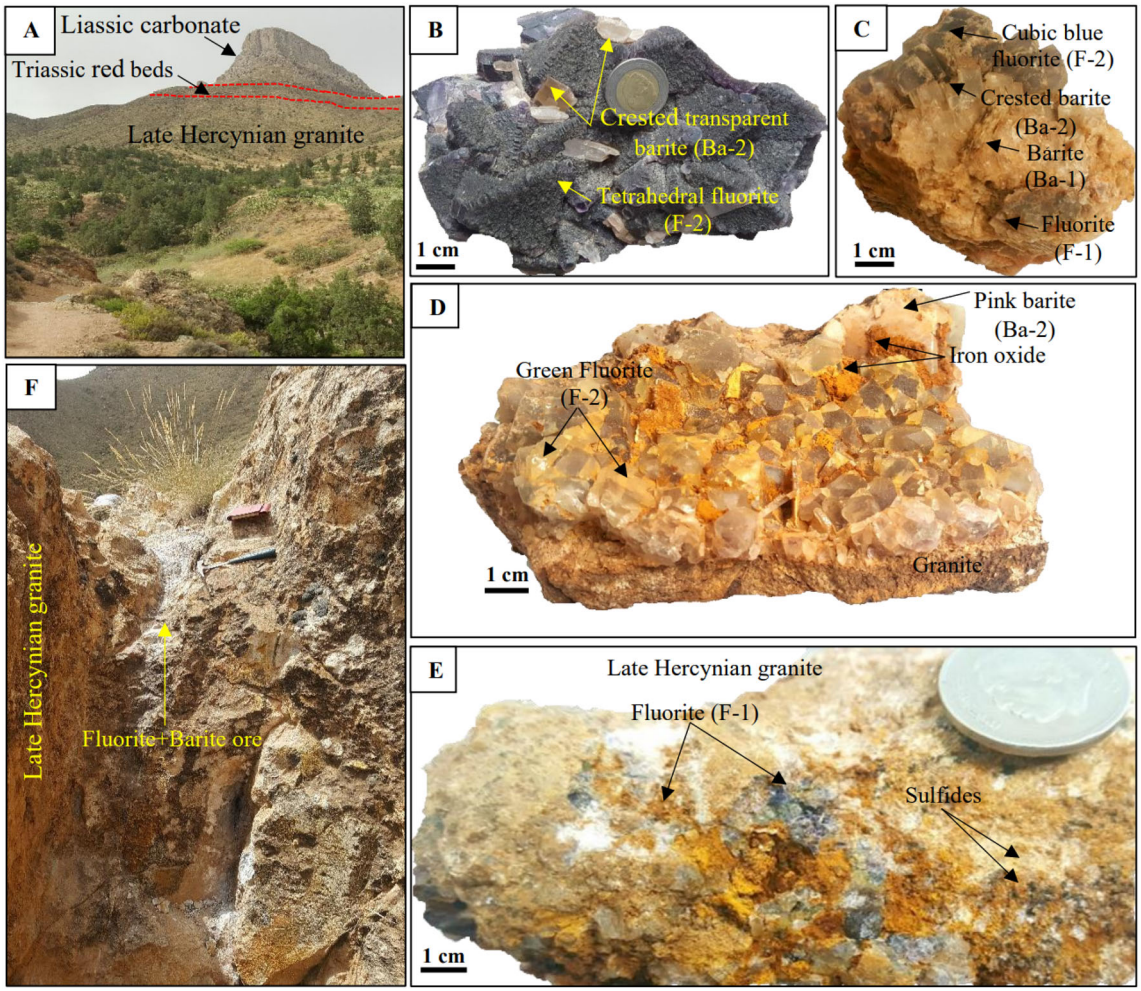

Fig. 3 Field photos and representative mineralized samples, show the main morphological types of fluorite barite mineralization in the Jbel Merguechoum. **A** Panoramic view of Jbel Merguechoum. **B** Specimen sample showing Tetratahedral purple fluorite (F 2) and the transparent lamellar barite (F 2). **C** Specimen sample showing the fluorine barite paragenetic succession of early ore stage (F 1 and Ba 1) and second ore stage (F 2 and Ba 2). **D** Ore sample in an open space ore style (vein in the Late Hercynian granite showing the paragenetic succession: cube green fluorine (F 2) massive barite (Ba 2) associated with iron oxides. **E** Substitution type mineralization (F 1 and sulfides) in the Late Hercynian granite. **F** Outcrop of an exploited fluorite barite vein in granite

the sample was taken up in 0.5 M HNO_3. To avoid co-dissolution of intergrown fluorite and quartz, the calcite samples were dissolved with 5 M HNO_3 in open PTFE beakers on a hotplate at ca. 70 80 °C, filtered and diluted to 0.5 M HNO_3 with deionized water. The samples were analyzed with a Spectro Ciros Vision ICP-OES and a Perkin Elmer Nexion 350×10 ppm Y (ICP-OES) and 1 ppb of Ru-Rh-Re-Bi (ICP-MS) were used for internal standardization. For quality control, the certified reference material JLs-1 (limestone; Geological Survey of Japan) was used. The results of the geochemical analyses are reported in Table 2. Barite is so insoluble even with strong acids that barite samples could not be prepared in wet chemistry. Hence, these barite samples were not analyzed for trace elements and REY.

Mineral separates of barite (Ba-1 and Ba-2) (n = 6) for sulfur and oxygen isotope analyses were handpicked under a binocular microscope. Sulfur and oxygen isotope analyses were carried out on barite samples at the spectrometry facility at the Department of Engineering, University of Nevada, Reno. These analyses were performed using a Eurovector elemental analyzer interfaced with a Micromass Isoprime stable isotope ratio mass spectrometer, after the methods of Giesemann et al. (1994) and Grassineau et al. (2001). The sulfur isotope compositions are expressed as $\delta^{34}S$ values relative to the V-CDT standard. Internal laboratory standards (sphalerite, marcasite) are used for calibrations (IAEA-S-1: $\delta^{34}S$ VCDT = − 0.3‰; IAEA-S-2: $\delta^{34}S$ VCDT = + 22.7‰. The analytical reproducibility was better than ± 0.2‰. For the oxygen isotope analyses,

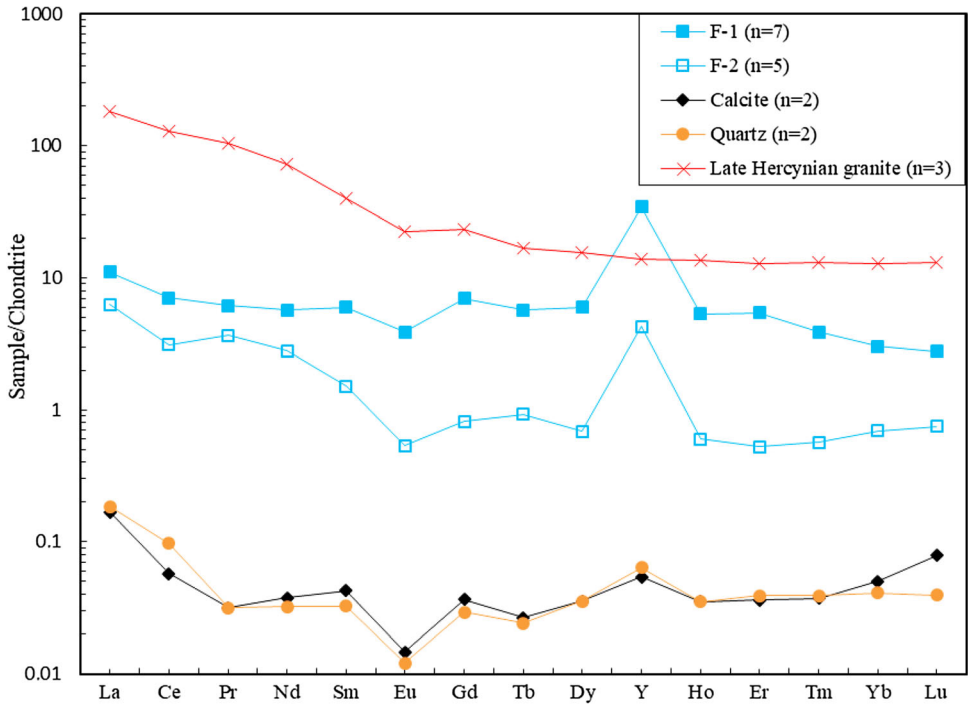

Fig. 4 Chondrite normalized REY patterns for fluorite 1, fluorite 2, calcite, quartz, and granite samples from the Jbel Merguechoum (see Table 2). The reference data of chondrite are from Taylor and McLennan (1985)

the IAEA-SO-5 ($\delta^{18}O$ SMOW = + 12.1‰), IAEA-SO-6 ($\delta^{18}O$ SMOW = − 11.3‰), and NBS-127 ($\delta^{18}O$ SMOW = + 8.8‰) were used as standards. The precision for oxygen analysis was better than ± 0.1‰.

4 Results

4.1 REY and trace elements geochemistry

The chondrite-normalized REY patterns (REY_{CN}) are illustrated in Fig. 4. The REY is normalized to chondrite (Taylor and McLennan 1985). The total REY contents (ΣREY) in early fluorite (F-1) range from 3.93 to 26.2 ppm (average: 16.3 ppm) and are higher than those of late fluorite (F-2) (ΣREY = 0.46 to 15.6 ppm, average: 6.0 ppm). Compared to fluorite, calcite and quartz samples display much lower ΣREY concentrations (0.08 11.7 ppm). The Late Hercynian granite exhibits higher REY concentrations (ΣREY avg. = 189 ppm) than the average ΣREY contents of other mineral phases. All fluorite samples are characterized by high LREY enrichment compared to HREY (Fig. 4) (LREY/HREY ratios often > 1 and $(La/Yb)_{CN}$ = 1.43 27.26) (Table 2). It is worth noting that the early fluorite is LREY-rich, whereas the late-stage fluorite is notably lower in LREY.

Fluorite of both stages (I and II) as well as calcite and quartz have low concentrations of incompatible high field strength elements (HFSE). In fluorite 1 and fluorite 2, the contents of thorium (Th) and uranium (U) are quite low, varying from 0.09 to 0.1 ppm and 0.07 to 0.2 ppm, respectively. Concerning the large ion lithophile elements (LILE), F-1 and F-2 display higher concentrations, especially barium (Ba). Particularly, green fluorite (F-1) and purple fluorite (F-1) have average Ba concentrations in the range of 59 3059 ppm, respectively. The concentrations of K, Sr, and Rb in both fluorites (F-1 and F-2) are variable, ranging from 30 to 100 ppm, 7 to 75 ppm, and 0.04 to 0.11 ppm, respectively. Nevertheless, the late fluorite (F-2) is most depleted in some elements (La, Ce, Nd, and Y). The Late Hercynian granite shows fairly high trace element contents (K, Ba, and Cs) and particularly potassium, with concentrations that reach up to 5.54% K.

The chondrite-normalized REY patterns of fluorite 1 and fluorite 2 are similar, but they are different from those of the post-ore calcite and quartz samples (Fig. 4). Conversely, the chondrite-normalized REY pattern of granite is completely different from that of fluorite and the post-ore calcite and quartz. The chondrite-normalized trace element diagrams show similar incompatible elements patterns of granite to those of fluorite, except for some elements, particularly Rb, K, and Ti (Fig. 5).

4.2 Eu, Ce, and Y anomalies

The Eu, Ce, and Y anomalies are calculated using the equations of Deng et al. (2014) (Table 2). Fluorite of both generations shows negative Eu anomalies with values of Eu/Eu* ratios less than 1 (0.25 0.72) (Table 2). These fluorite samples display a decreasing Eu/Eu* ratio from the

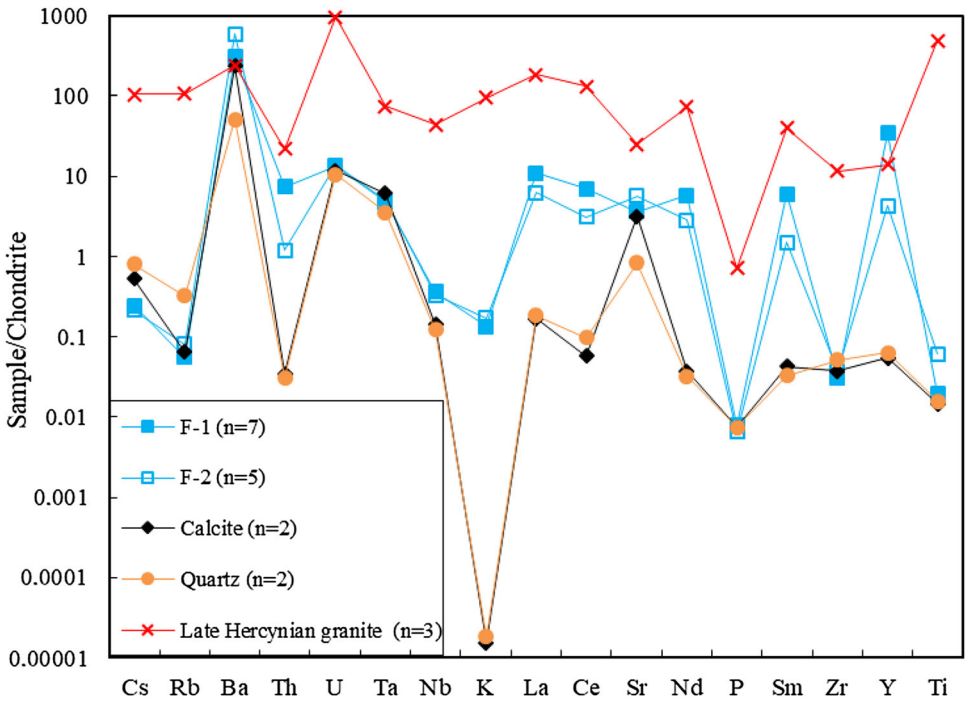

Fig. 5 Chondrite normalized trace element patterns for fluorite, calcite, quartz, and granite samples from the Jbel Merguechoum (see Table 2). The reference data of chondrite are from McDonough and Sun (1995)

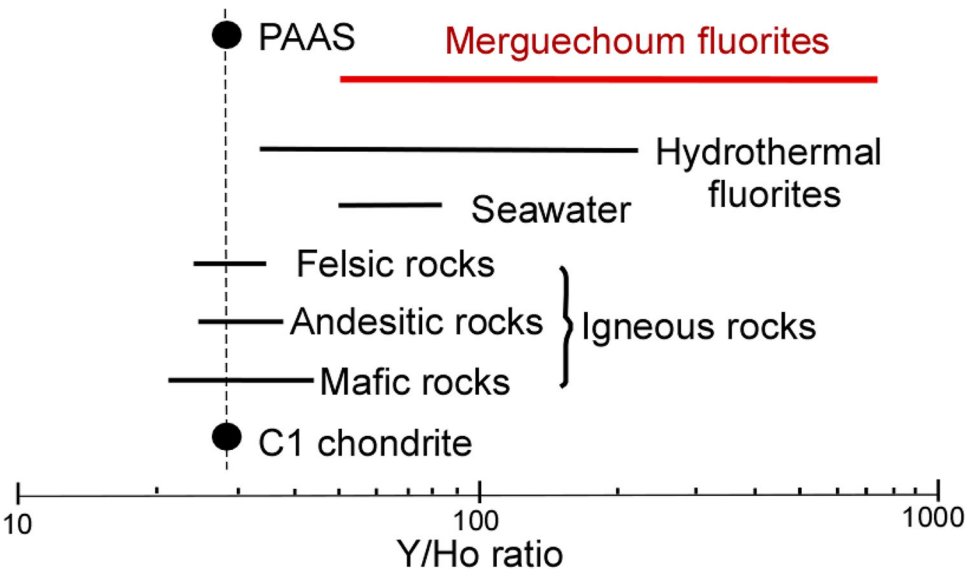

Fig. 6 Comparison of the Y/Ho ratios of Jbel Merguechoum fluorite. Igneous rocks, chondrite, PAAS (Post Archaean Australian Shale), and hydrothermal fluorite are also plotted for comparison (after Bau and Dulski 1995). PAAS data from Taylor and McLennan (1985)

early REY-enriched fluorite (F-1) (Eu/Eu* = 0.72) to the late REY-depleted fluorite (F-2) (Eu/Eu* = 0.25). All fluorite samples also display a negative Ce anomaly, with values of Ce/Ce* ratios ranging from 0.38 to 0.87 (Table 2). Interestingly, this fluorite also shows a decreasing Ce/Ce* trend from the early fluorite (F-1) (Ce/Ce* = 0.87) to late fluorite (F-2) (Ce/Ce* = 0.38). Fluorite samples show Y/Y* ratios ranging from 0.6 to 89.5 (Table 2). Early fluorite (F-1) has higher Y/Y* ratios than that late fluorite (F-2) (Table 2).

4.3 Y/Ho, La/Ho, Tb/La and Tb/Ca ratios

The analyzed fluorite of both generations exhibits a wide range of La/Ho values ranging from 1.17 to 50 as shown in Table 2. Conversely, these fluorite samples display a narrow range of Y/Ho ratios with average values varying between 255.4 in early fluorite and 156.2 in late fluorite (Fig. 6). Calcite and quartz samples have a wide range of La/Ho ratios (0.83 to 40.0) and Y/Ho ratios (40.0 to 141.7) (Table 2). The Late Hercynian granite record completely different La/Ho and Y/Ho ratios than those of fluorite (F-1, F-2), calcite, and quartz samples (La/Ho = 31.38 to 71.17,

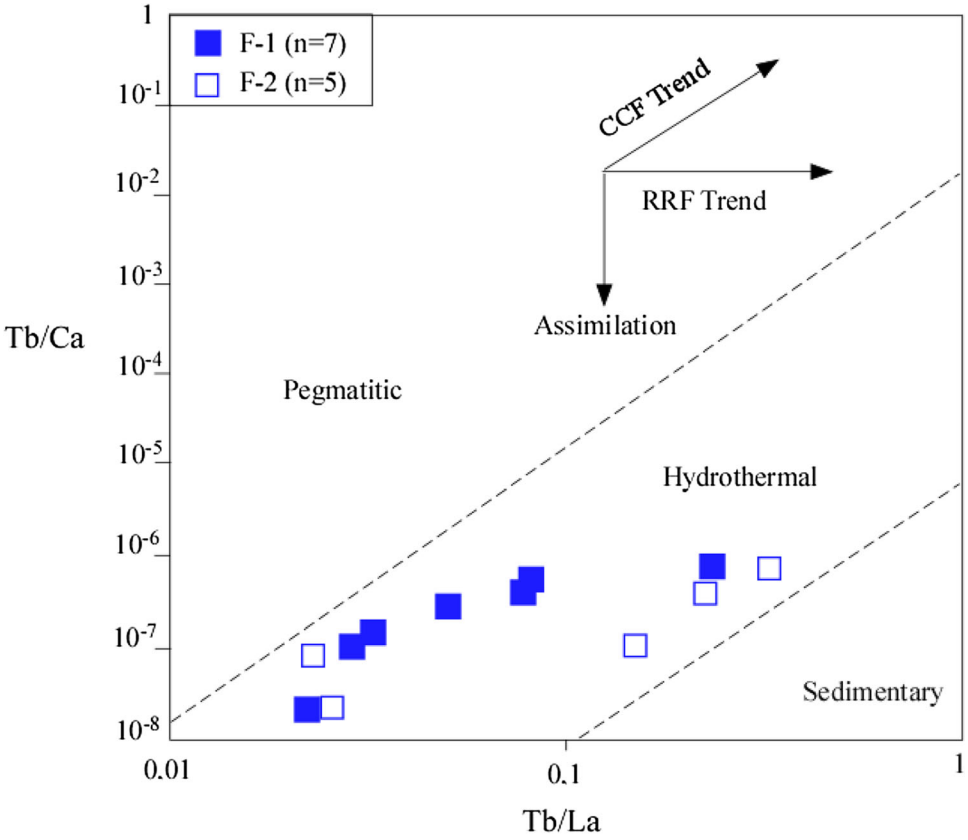

Fig. 7 Plots of Tb/Ca versus Tb/La ratios in fluorite from the Jbel Merguechoum. (CCF: crystal chemical; RRF: remobilization) (modified after Möller et al. 1976)

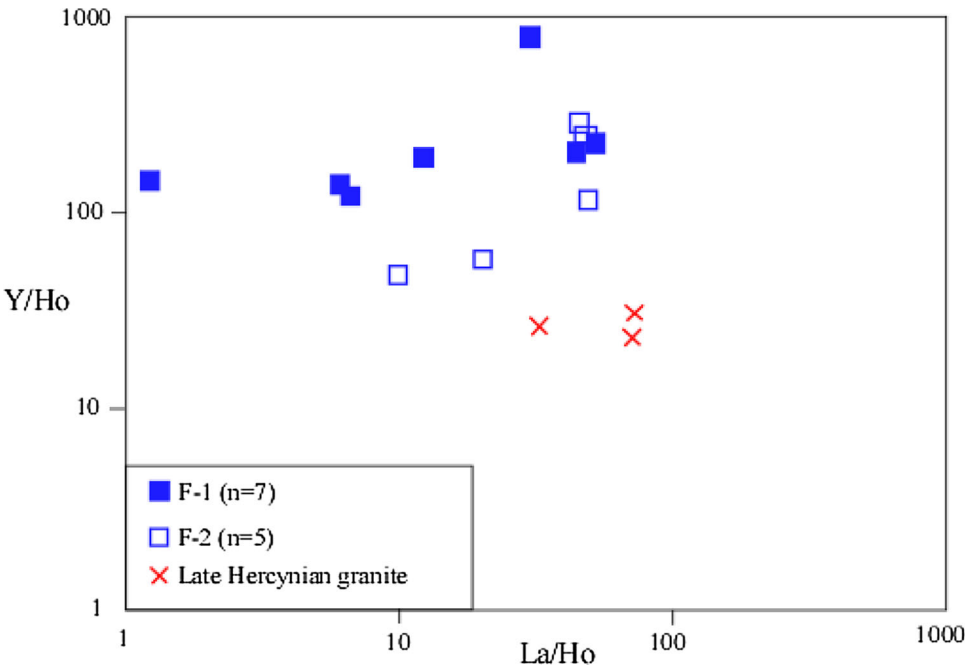

Fig. 8 Plots of Y/Ho versus La/Ho ratios in fluorite from the Jbel Merguechoum (modified after Bau and Dulski 1995)

Y/Ho = 25.33 to 33.50). Finally, the Tb/Ca and Tb/La ratios for all fluorite samples range from 0.02 to 0.9 and 3.6×10^{-8} to 1×10^{-6}, respectively.

4.4 Oxygen and sulfur isotopes

The sulfur and oxygen isotope compositions for barite samples are reported in Table 3. Barite samples of both

Table 3 Oxygen and sulfur isotopic compositions of various generations of barite from the Merguechoum fluorite barite hydrothermal vein system

Reference	Mineral	$\delta^{34}S$ (VCDT, ‰)	$\delta^{18}O$ (VSMOW, ‰)
MPBa 1	Massive pink barite 1	8.77	11.66
MPBa 2	Massive pink barite 2	8.82	11.20
MWBa 1	Massive white barite 1	8.93	12.46
MWBa 2	Massive white barite 2	8.87	11.98
CWBa 1	Crested white barite 1	8.82	12.18
CWBa 2	Crested white barite 2	8.61	11.81

generations display uniform S and O isotopic compositions with values ranging from 8.6 to 8.9 ‰ (avg. = 8.8 ‰) and 11.2 to 12.5 ‰ (avg. = 11.9 ‰), respectively. These isotopic values are close to those of the Permian seawater sulfates (i.e. $\delta^{34}S = 10.5 \pm 1.0$ ‰ and $\delta^{18}O = 10.97 \pm 0.29$ ‰) (Claypool et al. 1980; Strauss 1997). The $\delta^{34}S$ data of Merguechoum are also similar to those reported for the barite samples of the ore deposits of Aouli (8.6 to 13.4 ‰) (Margoum et al. 2015) and Jebilet (8.90 to 14.7 ‰) (Valenza et al. 2000).

5 Discussion

5.1 Age of the ore and source of the fluids

Although the absolute age of mineralization at Jbel Merguechoum cannot be determined accurately, geological and geochemical data allow us to constrain the age of fluorite-barite ore emplacement. The ore is hosted in fractures and faults that affect the Hercynian granite, suggesting that the ore post-dates the emplacement of granite. Hence, the ore must have formed after the crystallization of granite, thereby precluding the involvement of the magmatic/orthomagmatic fluids in the genesis of the ore. This conclusion is supported by the different REY patterns displayed by granite compared to those recorded for fluorite and barite samples. The fracturing and faulting of granite took place during the Permian Triassic rifting and the breakup of Pangea (Irving 1977; Torcq et al. 1997; Muttoni et al. 2003; Martins et al. 2008; Burisch et al. 2022). Hence, the fluorite-barite ore occurred during the Permian Triassic rifting event, which is known to be associated with the genesis of several ore deposits worldwide (Pirajno 2007; Burisch et al. 2022). This proposed age is similar to that suggested for the Aouli ore deposits (Margoum et al. 2015) and El Hammam (Bouabdellah et al. 2016; Lecumberri-Sanchez et al. 2018).

The Permian Triassic rifting resulted in the crust's extensional tectonic activity and subsequent thinning. This extensional tectonic activity and the related decompression of over-pressurized rocks remobilized and delivered a large amount of the deep-seated fluids toward shallow crustal levels as shown by the hydrological model set forth by Staude et al. (2009) and Bons et al. (2018) (see also Boiron et al. 2010; Burisch et al. 2016; Essarraj et al. 2017; Walter et al. 2019; de Graaf et al. 2020; Haschke et al. 2021; Rddad et al. 2022).

Fluids may have also migrated upward due to the exhumation of the mantle with the crustal thinning (Burisch et al. 2022; Rddad et al. 2022). The extension-related faults and fractures served as conduits for the upward migration of these deep-seated metalliferous fluids and the downwelling of the meteoric water.

5.2 Characterization of the ore-forming fluids

The Tb/La and Tb/Ca ratios of fluorite indicate the fractionation degree of hydrothermal fluids because the elements La and Tb are strongly fractionated by fluorite saturation (Ahmet et al. 2018). This Tb/La vs Tb/Ca diagram is, therefore, widely used to distinguish the physicochemical conditions and the environment of ore formation (pegmatitic, hydrothermal, or sedimentary) of fluorite (Möller et al. 1976; Möller and Morteani 1983). The investigated fluorite of both generations plotted in the hydrothermal field in the Tb/La vs Tb/Ca diagram (Fig. 7). Moreover, the values of the Y/Ho ratio of the studied fluorite samples vary from 50 to 731 (Table 2), which fall within those of hydrothermal fluorite (Fig. 6) according to Bau and Dulski (1995). Moreover, the REY source affects the REY concentrations in fluids, and it is known that the igneous rocks-derived fluids have overall much higher REY contents that those of the sedimentary rock-derived fluids (e.g. shale). In Merguechoum, fluorite and barite of both generations have low total REY contents, which suggests that these fluids are likely basinal brines which are

known to contain very low REY concentrations compared to the high-temperature magmatic-derived fluids (e.g. Nadoll et al. 2019a).

With regards to the transport of REY, F^-, SO_4^{2-}, and CO_3^{2-}/ HCO_3^- ions are possible ligands in the mineralizing fluids. Cl^- anions are also possible ligands of REY as they are efficient complexing agents (Migdisov et al. 2016; Migdisov 2019). The low solubility of barite limits the concentration of SO_4^{2-} anions in the ore-forming fluids, which suggests that these anions are not the main complexing ligands. The presence of calcite in the early and second ore events points to the possible contribution of CO_3^{2-}/HCO_3^- ions as complexing agents. Fluorite samples (F-1 and F-2) display a positive Y anomaly and have Y/Ho ratios of 50 to 731 greater than those of the chondrite (Y/Ho ratios = 28; Anders and Grevesse 1989), indicating the higher stability of the Y-F complexation compared to that of the Ho-F (Bau 1996). Positive Y anomaly also suggests the presence of fluoride complexing agents (Möller 1998), which is in agreement with the preferential incorporation of yttrium into fluorite in hydrothermal fluids (Deng et al. 2014). Based on the aforementioned arguments, it is concluded that F^-, CO_3^{2-}/ HCO_3^- ions, and possibly Cl^- anions are the main transporting agents with a contribution of other complexing agents such as SO_4^{2-}).

5.3 Source of sulfur and oxygen isotopes in barite

The sulfur and oxygen isotope compositions of the Merguechoum barite samples are uniform and are closer to those of the Permian Triassic seawater (Claypool et al. 1980; Strauss 1997). Hence, barite samples share a similar dissolved sulfate source which is likely the Permian Triassic seawater and/or pore-seawater sulfate. The metalliferous Ba-rich ascending fluid cannot carry sulfates owing to the low solubility of Ba (solubility product $K_{SP} = [Ba^{2+}][SO_4^{2-}] = 10^{-10}$) in SO_4^{2-}-rich fluid. Therefore, this low solubility constraint on Ba concentration implies that the deep-seated fluid transported metals, whereas SO_4^{2-} anions were supplied by the Permian Triassic seawater and/or pore-seawater. The ascending Ba-enriched ore fluids encountered and mixed with these SO_4^{2-}-rich Permian Triassic-derived descending fluids, leading to the precipitation of barite.

5.4 Evolution of the ore-forming fluids

Several studies showed that fluorite displays REY fractionation between LREY and HREY, which is used to decipher the redox and Physico-chemical conditions that prevailed during fluorite deposition (Bau and Möller 1992; Bau and Dulski 1995; Ehya 2012; Schwinn and Markl 2005). The variations in ΣREY contents and REY fractionation observed in the different types of fluorite generations are related to the evolution of the Physico-chemical conditions (pH, fO_2, Temperature) conditions of the mineralizing fluids. Particularly, the LREY-rich early fluorite suggests high temperatures under slightly acidic conditions (e.g. Ehya 2012) during the precipitation of F-1. Conversely, the LREY-depleted late-stage fluorite likely reflects alkaline conditions in the presence of carbonate species (Chen and Zhao 1997; Ehya 2012; Deng et al. 2014; Schwinn and Markl 2005) during the precipitation of F-2.

The Eu/Eu* and Ce/Ce* ratios also provide information on the Physico-chemical conditions of hydrothermal fluids, including temperature, pH, and oxygen fugacity (Bau and Möller 1992; Möller 1998; Bau and Dulski 1995; Schwinn and Markl 2005). The observed negative Eu anomalies in fluorite samples (F-1 and F-2) are probably inherited from granite (Schwinn and Markl 2005) where Eu is located in the mineral structure of plagioclase rather than the rock groundmass and crystal rims where the other REY is located. The REY patterns of fluorite samples are indicative of intense water rock interaction with granite during the precipitation of fluorite 1. This water rock interaction of the first ore stage mobilizes the REY pool first, creating the Eu-depleted REY patterns. Fluorite samples of ore stage 2 have an overall lower ΣREY concentration, which could suggest i) REY-depleted fluid due to the precipitation of F-1 and ii) less intense fluid-rock interaction due to lower temperatures. The former explanation is valid given the obvious removal of REY from the ore-forming fluids of the first stage and subsequent depletion of the fluids of the second stage. The second explanation is also reasonable because there is an increase in the influx of meteoric water that cooler the hydrothermal system as evidenced by the observed decreasing Ce/Ce* and Eu/Eu* anomalies. Indeed, the increase of the meteoric water in the hydrothermal system had cooled and diluted the ore-forming fluid, causing a slight decrease in total REY content from the early ore stage to the second ore stage. The post-ore calcite and quartz samples show further REY depletion, which could be explained by the two above-mentioned proposed scenarios: (i) a dilution of the metalliferous fluid by meteoric water and (ii) a decrease in fluid-rock interaction.

5.5 Source of metals

It is generally known that the migrating mineralizing brines along different rocks results in the leaching of the metals, including F and Ba from the country rocks (e.g. Leach et al. 2005; Yardley 2005; Margoum et al. 2015; Walter et al. 2019; Burisch et al. 2016; Haschke et al. 2021). At Merguechoum, the potential source rocks for these elements

include the metamorphic and igneous rocks of the Hercynian crystalline basement, including the Late Hercynian granite. The similar patterns of all Merguechoum fluorite samples (F-1 and F-2) in the chondrite-normalized trace element diagrams (Fig. 5) suggest a common source for these fluorites. The similar patterns of the incompatible elements of the Hercynian granite and fluorite samples suggest that the source of F in fluorite is granite, particularly from the breakdown of mica. Moreover, the elevated concentrations of barium (Ba) in fluorite, due to a similarity in ion radii between calcium (Ca) and barium (Ba) (Dai 1987), suggests that the metal-bearing fluids are rich in Ba which is particularly derived from the dissolution of feldspar. REY and trace element data of both the ore and granite reveal fluid-rock interaction between the metalliferous fluids and granite. The duration of this fluid-granite interaction is relatively longer as revealed by the relatively moderate positive correlation between the La/Ho and Y/Ho ratios observed for fluorite 1 and fluorite 2 (Fig. 8). The circulation of the mineralizing fluids in the intensely fractured granite may have, hence, leached elements including F and Ba from granite.

Moreover, the LILE and HFSE concentrations in the mineralization are controlled by the physicochemical conditions of hydrothermal fluids and the geological environment (Möller et al. 1976; Bau et al. 2003; Sasmaz et al. 2005a, b; Schwinn and Markl 2005; Sasmaz and Yavuz 2007; Schönenberger et al. 2008; Sanchez et al. 2010; Souissi et al. 2010; Ehya 2012; Akgul 2015; Alipour et al. 2015; Azizi et al. 2017). In that respect, the enrichment of fluorite and granite in LILE can be explained by the fact that these elements migrate easily with the hydrothermal fluids (Bau and Möller 1992; Schwinn and Markl 2005). This is not the case for HFSE which has little or no mobility in the hydrothermal fluids (Bau and Möller 1992; Schwinn and Markl 2005), which resulted in a depletion of these elements in fluorite. These geochemical characteristics allow the classification of granite (the host rock) in the strongly potassic calc-alkaline granitoid. This is corroborated by the high La/Nb ratios that are always higher than 2 (average La/Nb $\approx$ 3.94). The leaching of this K-rich granite by the ore-bearing fluids explained the enrichment of fluorite in potassium among other elements. This observation further supports the fluid-granite interaction that took place during the circulation of the ore-forming fluids and their subsequent trace element enrichment. It follows that the Late Hercynian granite is a major contributor of fluorite and barite required for the precipitation of fluorite and barite.

5.6 Mechanisms of the ore precipitation

The processes that trigger the precipitation of fluorite and barite are (i) the mixing of two or more fluids of different chemical compositions, (ii) precipitation due to the decreasing temperature and pressure of the metalliferous fluid, and (iii) the fluid-rock interaction (e.g. Richardson and Holland 1979; Roedder 1984; Simonetti and Bell 1995). Precipitation of barite and fluorite require the aforementioned factors (i-iii) owing to the low solubility of barite (Hanor 2000) and the notable decrease in the solubility of F with decreasing temperature (Richardson and Holland 1979). At Merguechoum, the mineralized veins crosscut the Late Hercynian granite and hence, the magmatic fluid is excluded because the ore must have precipitated well after the crystallization of granite. This conclusion is consistent with the different REY patterns of fluorite samples (F-1 and F-2) compared to those of the Hercynian granite samples. These observations exclude a direct genetic relation between granite and mineralization; that is the magmatic-derived fluids are not involved in the genesis of the ore. A similar disconnect between the ore and the Hercynian granitic magma is observed for the fluorite-barite ore deposits of El Hammam (Bouabdellah et al. 2016) and Aouli (Margoum et al. 2015). REY data indicate that the basinal brines are involved in the genesis of the ore with the involvement of meteoric water. It is likely that fluid mixing between the metal-rich basinal brines and diluted, cooler, sulfate-rich meteoric water occurred, triggering the precipitation of fluorite and barite. The similar REY patterns of fluorite 1 and fluorite 2 show that these mineral phases precipitated by mixing from those same fluid endmembers. Moreover, fluorite samples have a high concentration of Ba, which suggest that F and Ba were transported in the same hydrothermal fluids.

Fluid-mixing has been proposed as a primary process in the precipitation of F and Ba in several ore deposits that formed with Pangea rifting (North Africa: Aouli, Margoum et al. 2015; El Hammam, Bouabdellah et al. 2016; Europe: Grandia et al. 2003; Boiron et al. 2010; Kraemer et al. 2019; Walter et al. 2019; Nadoll et al. 2019a; Guilcher et al. 2021; Burisch et al. 2022; North America: Van Alstine 1976).

Compared to the early ore stage, the coarse euhedral texture of fluorite 2 and barite 2 suggests very fast precipitation of these minerals during fluid mixing under supersaturation conditions. In that respect, modeling set forth by Walter et al. (2018) shows that fluorite precipitates within seconds. The oscillatory zoning exhibited by F-1 suggests cyclic compositional fluctuation of the ore-forming fluids during early-stage ore. Each zone may reflect a single fluid batch expelled during seismic activity for example.

The high concentrations of Ba in granite and fluorite samples as well as trace elements and REY data indicate that fluid-rock interaction took place between the Hercynian granite and the ore-forming fluids. This fluid-rock interaction likely contributed to the precipitation of the ore besides the fluid-mixing process. Fluid-rock interaction was intense during the first ore stage compared to that of the second ore stage (refer to Sect. 5.4).

The source of calcium, required for fluorite precipitation, could be i) the albitization of plagioclase in the Late Hercynian granite, ii) the dissolution and leaching of the Triassic feldspars, and iii) the dissolution of the Hercynian granite and Liassic carbonate. The lack of a positive Eu anomaly in fluorite samples discounts the first two former sources of Ca. The high concertation of Ca in the Late Hercynian granite (2700 15,200 ppm) points to the latter as one possible contributor to Ca input. The juxtaposition of the Liassic rocks to the ore sites may suggest that Ca was also derived from the dissolution of the Liassic carbonate and probably brought to the loci of deposition. However, based on the oxygen isotope data, the sulfates of barite samples derived from the Permian seawater and/or coeval pore-seawater, preclude the Liassic carbonate as the source of calcium. This conclusion is also in agreement with the proposed Permian Triassic age of the ore genesis during which similar ore deposits were formed (e.g., Aouli, Margoum, et al. 2015; El Hammam, Bouabdellah, et al. 2016; Muchez et al. 2005; Haschke et al. 2021; Burisch et al. 2022).

6 Ore genesis and concluding remarks

The fluorite-barite veins of the Jbel Merguechoum, hosted in the Late Hercynian granite, are structurally controlled. The paragenesis consists of fluorite 1- fluorite 2- barite 1- barite 2 -calcite with a subordinate amount of quartz, chalcopyrite, pyrite, and supergene mineral assemblage. Three main ore stages are identified: i) early hydrothermal stage, ii) second hydrothermal "Euhedral" stage, and iii) supergene "post-ore stage". The geochemical analyses of trace elements (REY, HFSE, and LILE) in fluorite and barite of the Jbel Merguechoum reveal that the hydrothermal basinal brines are involved in the precipitation of fluorite with the involvement of meteoric water. Based on the geological and geochemical data, we suggest that the ore-forming basinal brines migrated from a deep part of the basin along the deep-seated Hercynian NE-SW to ENE-WSW-trending faults. These faults were formed in response to the crustal thinning during Pangea rifting. Sedimentary basinal brines were also proposed as the ore-forming fluids for the Fluorite-barite ore deposits of Aouli (Margoum et al. 2015) and El Hammam (Bouabdellah et al. 2016). Along their ascent to the loci of deposition along potential pathways, these basinal fluids interacted with the Paleozoic rocks, including the Late Hercynian granite, and scavenged the elements (e.g., REY, F, and Ba). The mixing between these deep-seated metalliferous basinal brines and cooler, diluted sulfate-rich meteoric water triggered the precipitation of F-1 from REY-enriched hydrothermal fluids. The increasing influx of meteoric water cooled and diluted the hydrothermal system, which led to the deposition of F-2 from REY-depleted hydrothermal fluids in a less acidic, oxygenated environment. Fluid-rock interactions between the ore-forming fluids and the Late Hercynian granite have not only enriched these fluids in elements (e.g., REY, F, Ba) but also contributed to the precipitation of the ore. REY data show that fluid-rock interaction is pronounced during the first ore stage compared to the second ore stage, explaining the higher REY contents in F-1 and Ba-1. Furthermore, the removal of REY by the minerals of the first ore stage 1 leads to REY depletion of the ore-forming fluids of the second stage.

The Mechergoum ore deposits share similarities with several ore deposits that are formed to the Permian Triassic rifting (North Africa: Margoum et al. 2015; El Hammam, Bouabdellah, et al. 2016), Europe (e.g. Muchez et al. 2005; Haschke et al. 2021; Burisch et al. 2022 and references therein). Future studies (e.g. fluid inclusions, crush-leach, Sr isotopes) will be performed to further constrain the nature and evolution of the ore-forming fluids and consolidate the genetic ore model presented in this paper.

Acknowledgements We would like to express our gratitude to Dr. Dennis Kraemer, Dr. David Lentz, and an anonymous reviewer for their constructive and insightful comments that improve the quality of this manuscript. We also thank the Managing Editor, Dr. Binbin Wang, for handling our paper.

Declarations

Conflict of interest The authors declare that they have no conflict of interest.

References

Akgul B (2015) Geochemical associations between fluorite mineral ization and A type shoshonitic magmatism in the Keban Elazig area, East Anatolia, Turkey. J Afr Earth Sci 111:222 230

Alipour S, Abedini A, Talaei B (2015) Geochemical characteristics of the Qahr Abad fluorite fluorite deposits, south east of Saqqez, western Iran. Arab J Geosci 8:7309 7320

Alles J, Ploch A M, Schirmer T, Nolte N, Liessmann W, Lehmann B (2019) Rare earth element enrichment in post Variscan poly metallic vein systems of the Harz Mountains, Germany. Miner Deposita 54:307 328

Azizi MR, Abedini A, Alipour S, Niroomand S, Sasmaz A, Talaei B (2017) Rare earth element geochemistry and tetrad effect in

fluorites: a case study from the Qahr Abad deposit. Iran N Jb Palont 283(3):255 273

Bau M, Dulski P (1995) Comparative study of yttrium and rare earth element behaviours in fluorine rich hydrothermal fluids. Contrib Mineral Petrol 119:213 223

Bau M, Dulski P (1996) Distribution of yttrium and rare earth elements in the Penge and Kuruman iron formations, Transvaal Supergroup, South Africa. Precambrian Res 79:37 55

Bau M, Möller P (1992) Rare earth element fractionation in metamorphogenic hydrothermal calcite, magnesite and siderite. Miner Petrol 45:231 246

Bau M, Romer RL, Lüders V, Dulski P (2003) Tracing element sources of hydrothermal mineral deposits: REE and Y distribu tion and Sr Nd Pb isotopes in fluorite from MVT deposits in the Pennine Orefield, England. Miner Deposita 38:992 1008

Berrada Hmima Y (1993) Magmatisme séquentiel des massifs de Tanncherfi et de Merguechoum. Terminaison orientale de la chaîne hercynienne du Maroc. Thèse 3ème cycle, Université Cadi Ayyad, Faculté des Sciences Semlalia, Marrakech, Maroc, p 144 (in French)

Boiron MC, Cathelineau M, Richard A (2010) Fluid flows and metal deposition near basement/cover unconformity: lessons and analogies from Pb Zn F Ba systems for the understanding of Proterozoic U deposits. Geofluids 10(1 2):270 292

Bouabdellah M, Zemri O, Jébrak M, Klügel A, Levresse G, Maacha L, Gaouzi A, Souiah M (2016) Geology and mineralogy of the El hammam REE rich fluorite deposit (Central Morocco): a product of transtensional Pangean Rifting and Central Atlantic Opening. In: Bouabdellah M, Slack JF (eds) Mineral deposits of north Africa. Springer International Publishing, Cham, pp 307 324. https://doi.org/10.1007/978 3 319 31733 5 12

Burisch M, Walter BF, Wälle M, Markl G (2016) Tracing fluid migration pathways in root zone below unconformity related hydrothermal veins: Insights from trace element systematics of individual fluid inclusions. Chem Geol 429:44 50

Burisch M, Markl G, Gutzmer J (2022) Breakup with benefits hydrothermal mineral systems related to the disintegration of a supercontinent. Earth Planet Sci Lett 580:117373

Chen YJ, Zhao YC (1997) Geochemical characteristics and evolution of REE in the early Precambrian sediments: evidences from the southern margin of the North China craton. Episodes 20:109 116

Chotin P, Ait Brahim L, Tabyaoui H (2000) The Southern Tethyan margin in Northeastern Morocco; sedimentary characteristics and tectonic control. Mémoires du Muséum national d'histoire naturelle 182:107 127.Clauer N, Jeannette D, Tisserant D (1980) Datations isotopiques des cristallisations successives d'un socle hercynien et cristallophyllien (Haute Moulouya, Moyen Maroc). Geol Rundsch 69:63 83

Claypool GE, Holser WT, Kaplan TR, Sakai H, Zak I (1980) The age curves of sulfur and oxygen isotopes in marine sulfate and their mutual interpretations. Chem Geol 28:199 260

Dai AB (1987) Coordination chemistry. Science Publication, Beijing

De Graaf S, Lüders V, Banks DA, Sośnicka M, Reijmer JJG, Kaden H, Vonhof HB (2020) Fluid evolution and ore deposition in the Harz Mountains revisited: isotope and crush leach analyses of fluid inclusions. Miner Deposita 55:47 62

Deng XH, Chen YJ, Yao JM, Bagas L, Tang HS (2014) Fluorite REE Y (REY) geochemistry of the ca. 850 Ma Tumen molybdenite fluorite deposit, eastern Qinling, China: constraints on ore genesis. Ore Geol Rev 63:532 543

Ehya F (2012) Variation of mineralizing fluids and fractionation of REE during the emplacement of the vein type fluorite deposit at Bozijan, Markazi province. Iran J Geochem Explor 112:93 106

Hadi EL, H, Tahiri A, Reddad A, (2003) Les granitoïdes hercyniens post collisionnels du Maroc oriental: une province magmatique calco alcaline à shoshonitique. C R Geosci 335:959 967 (**in French**)

Gasquet D, Stussi J, Nachit H (1996) Les granitoïdes hercyniens du Maroc dans le cadre de l'évolution géodynamique régionale. Bull Soc Géol France 167(4):517 528 (**in French**)

Giesemann A, Jäger HJ, Norman AL, Krouse HR, Brand WA (1994) Online sulfur isotope determination using an elemental analyzer coupled to a mass spectrometer. Anal Chem 66(18):2816 2819

Giret P (1985) Histoire paléogéographique, pétrographique et struc turale du district à fluorine de Taourirt (Maroc Oriental). Thèse 3ème cycle, Orléans, p 191, (in French)

Grassineau NV, Mattey DP, Lowry D (2001) Sulfur isotope analysis of sulfide and sulfate minerals by continuous flow isotope ratio mass spectrometry. Anal Chem 73(2):220 225

Guilcher M, Albert R, Gerdes A, Gutzmer J, Burisch M (2021) Timing of native metal arsenide (Ag Bi Co Ni As±U) veins in continental rift zones In situ U Pb geochronology of carbonates from the Erzgebirge/Krušné Hory province. Chem Geol 584:120476

Hanor JS (2000) Barite celestite geochemistry and environments of formation. Rev Mineral Geochem 40:193 263

Haschke S, Gutzmer J, Wohlgemuth Ueberwasser CC, Kraemer D, Burisch M (2021) The Niederschlag fluorite (barite) deposit, Erzgebirge/Germany a fluid inclusion and trace element study. Miner Deposita 56:1071 1086

Hoepffner C, Soulaimani A, Piqué A (2005) The moroccan hercynides. J Afr Earth Sci 43:144 165

Hoepffner C (1987) La tectonique hercynienne dans l'Est du Maroc. Thèse de doctorat Université Louis Pasteur, p 276, (in French)

Hollard Henri (1978) L'Evolution hercynienne au Maroc. Zeitschrift der Deutschen Geologischen Gesellschaft 129(2):495 512. https://doi.org/10.1127/zdgg/129/1978/495

Huon S, Cornée JJ, Piqué A, Rais N, Clauer N, Liewig N, Zayane R (1987) Mise en évidence au Maroc d'événements thermiques d'âge triasico liasique liés à l'ouverture de l'Atlantique. Bull Soc Géol France 164:165 176 (**in French**)

Kraemer D, Viehmann S, Banks D, Sumoondur AD, Koeberl C, Bau M (2019) Regional variations in fluid formation and metal sources in MVT mineralization in the Pennine Orefield, UK: implications from rare earth element and yttrium distribution, Sr Nd isotopes and fluid inclusion compositions of hydrothermal vein fluorite. Ore Geol Rev 107:960 972

Lagard JL (1989). Granite tardi carbonifère et déformation crustale. EXEMPLE de la Meseta marocaine. Mémoires et documents du C A.E.S.S. n 26, Renne, p 353 (in French)

Lecumberri Sanchez P, Bouabdellah M, Zemri O (2018) Transport of rare earth elements by hydrocarbon bearing brines: Implications for ore deposition and the use of REEs as fluid source tracers. Chem Geol 479:204 215

Margoum D, Bouabdellah M, Klügel A, Banks DA, Castorina F, Cuney M, Jébrak M, Bozkaya G (2015) Pangea rifting and onward pre Central Atlantic opening as the main ore forming processes for the genesis of the Aouli REE rich fluorite barite vein system, upper Moulouya district, Morocco. J Afr Earth Sci 108:22 39

Migdisov A, Williams Jones E, Brugger J, Caporuscio FA (2016) Hydrothermal transport, deposition, and fractionation of the REE: experimental data and thermodynamic calculations. Chem Geol 439:13 42

Möller P (1998) Europium anomalies in hydrothermal minerals, kinetic versus thermodynamic interpretation. In: Proceedings of the ninth quadrennial iagod symposium Schweizerbart, Stuttgart, pp 239 246

Möller P, Morteani G (1983) On the chemical fractionation of REE during the formation of Ca minerals and its application to problems of the genesis of ore deposits. In: Augustithis S (ed)

The significance of trace elements in solving petro genetic problems. Theophrastis Publishers, Athens, pp 747 791

Möller P, Parekh PP, Schneider HJ (1976) The application of Tb/Ca Tb/La abundance ratios to problems of flourspar genesis. Miner Deposita 11:111 116

Mrini Z, Rafi A, Duthou JL, Vidal P (1992) Chronologie Rb/Sr des granitoïdes hercyniens du Maroc, conséquences. Bull Soci Géol France 163(3):281 291 (**in French**)

Nadoll P, Sośnicka M, Kraemer D, Duschl F (2019a) Post Variscan structurally controlled hydrothermal Zn Fe Pb sulfide and Flu orite barite mineralization in deep seated Paleozoic units of the North German Basin: a review. Ore Geol Rev 106:273 299

Pirajno F (2007) Mantle plumes, associated intraplate tectonomag matic processes and ore systems. Episodes J Int Geosci 30(1):6 19

Rddad L, Kraemer D, Walter BF, Darling R, Cousens B (2022) Unravelling the fluid flow evolution and precipitation mecha nisms recorded in calcite veins in relation to Pangea rifting Newark Basin, USA. Geochemistry 82(4):125918

Richardson CK, Holland HD (1979) Fluorite deposition in hydrother mal systems. Geochim Cosmochim Acta 43(8):1327 1335

Roedder E (1984) Fluid inclusions. Washington DC mineral soc. Am Rev Mineral 12:1 644

Sasmaz A, Önal A, Sagıroğlu A, Önal M, Akgül B (2005a) Origin and nature of the mineralizing fluids of thrust zone fluorites in Celikhan (Adıyaman, Eastern Turkey): a geochemical approach. Geochem J 39:131 139

Sasmaz A, Yavuz F (2007) REE geochemistry and fluid inclusion studies of fluorite deposits from the Yaylagzü area (Yıldızeli Sivas) in central Turkey. N Jb Geol Paläont 183:215 226

Sasmaz A, Yavuz F, Sağıroğlu A, Akgül B (2005b) Geochemical patterns of the Akdağmadeni (Yozgat, Central Turkey) fluorite deposits and implications. J Asian Earth Sci 24:469 479

Schönenberger J, Köhler J, Markl G (2008) REE systematics of fluorides, calcite and siderite in peralkaline plutonic rocks from the Gardar Province, South Greenland. Chem Geol 247:16 35

Schwinn G, Markl G (2005) REE systematics in hydrothermal fluorite. Chem Geol 216:225 248

Simonetti A, Bell K (1995) Nd, Pb, and Sr isotope systematics of fluorite at the Amba Dongar carbonatite complex, India; evidence for hydrothermal and crustal fluid mixing. Econ Geol 90(7):2018 2027. https://doi.org/10.2113/gsecongeo.90.7.2018

Souissi F, Souissi R, Dandurand JL (2010) The Mississippi valley type (MVT) fluorite ore at Jebel Stah (Zaghouan District, northeastern Tunisia): contribution of REE and Sr isotope geochemistries to the genetic model. Ore Geol Rev 37:15 30

Strauss H (1997) The isotopic composition of sedimentary sulfur through time. Paleogeogr Paleoclimatol Paleoecol 132:97 118

Torbi A, Gélard J P (2000) Paléocontraintes identifiées dans la couverture méso cénozoïque du Maroc nord oriental. Relations avec l'ouverture de l'Atlantique et le rapprochement Afrique Europe. Comptes Rendus de l'Académie des Sciences Series IIA Earth and Planetary Science 330(12):853 858. https://doi.org/10.1016/S1251 8050(00)00227 5

Van Alstine RE (1976) Continental rifts and lineaments associated with major fluorspar districts. Econ Geol 71(6):977 987. https://doi.org/10.2113/gsecongeo.71.6.977

Valenza K, Moritz R, Mouttaqi A, Fontignie D, Sharp Z (2000) Vein and karst barite deposits in the western jebilet of Morocco: fluid inclusion and isotope (S, O, Sr) evidence for regional fluid mixing related to central Atlantic rifting. Econ Geol 95:587 606

Walter BF, Kortenbruck P, Scharrer M, Zeitvogel C, Wälle M, Mertz Kraus R, Markl G (2019) Chemical evolution of ore forming brines Basement leaching, metal provenance, and the redox link between barren and ore bearing hydrothermal veins. a case study from the Schwarzwald mining district in SW Germany. Chem Geol 506:126 148

Yardley BWD (2005) 100th anniversary special paper: metal concentrations in crustal fluids and their relationship to ore formation. Econ Geol 100:613 632

McDonough WF, Sun SS (1995) The composition of the Earth. Chem Geo 120(3 4): 223 253